PostPrint. Zikang Qin, et al., Separation and Purification Technology, 330 (2024) 125308
https://doi.org/10.1016/j.seppur.2023.125308

Thin film nanocomposite membranes fabricated via 2D ZIF-67 nanosheets and 1D nanofibers with ultrahigh water flux for dye removal from wastewater

Zikang Qin[a], Siying Xiang[a], Ziheng Jing[b,c,d], Ming Deng[a], Wenju Jiang[b,c,d], Lu Yao[b,c,d], Lin Yang[b,c,d], Liyuan Deng[e] and Zhongde Dai[b,c,d*]

[a]College of Architecture and Environment, Sichuan University, Chengdu 610065, China

[b]College of Carbon Neutrality Future Technology, Sichuan University, Chengdu 610065, China

[c]National Engineering Research Centre for Flue Gas Desulfurization, Chengdu 610065, China

[d]Carbon Neutral Technology Innovation Center of Sichuan, Chengdu 610065, China

[e]Department of chemical engineering, Norwegian University of Science and Technology, Trondheim, 7491, Norway

*Corresponding author:

Zhongde Dai, E-mail: zhongde.dai@scu.edu.cn

Abstract:

Thin-film nanocomposite (TFN) membranes based on metal-organic frameworks (MOFs) have received increasing attention in the field of water treatment. However, TFN membranes with both high permeance and rejection rates are highly desired. In this study, ultra-thin ZIF-67 was synthesized and TFN membranes were fabricated by combining the obtained 2D ZIF-67 with cellulose nanofibers (CNF) and carbon nanotubes (CNTs). The nanofibers not only fill the gaps between the ZIF-67 nanosheets but also form an intercalation layer between the ZIF-67 nanosheets and function as a water transport pathway, leading to a significant enhancement of water permeance. By introducing CNF into the ZIF-67-embedded matrix, the dye rejection rates increase to 96.8% and 93.3%, respectively, with water permeance of about 90.0 $L \cdot m^{-2} \cdot h^{-1} \cdot bar^{-1}$. Further introducing CNT into the CNF/ZIF-67 membrane further improved the water permeance to 207.8 $L \cdot m^{-2} \cdot h^{-1} \cdot bar^{-1}$, while a dye rejection rate of 95.1% was documented. The results indicate that the introduction of nanofibers into 2D MOF matrix to form TFN membranes has great potential for wastewater treatment.

Keywords:

Thin-film nanocomposite membranes; 2D MOF; nanocellulose fibers, carbon nanotubes; wastewater treatment

Highlights:

- Ultra-thin (<50nm) 2D hexagonal ZIF-67;
- Novel TFN membranes fabricated via 2D ZIF 67 and two types of nanofibers were developed;
- Two types of nanofibers play different roles in membranes;
- Incorporating 2 fibers into the ZIF-67 further enhanced water permeance to over 200.0 $L \cdot m^{-2} \cdot h^{-1} \cdot bar^{-1}$ with a dye rejection rate of 95.1%
- The obtained TFN membranes demonstrated excellent long-term stability.

TOC:

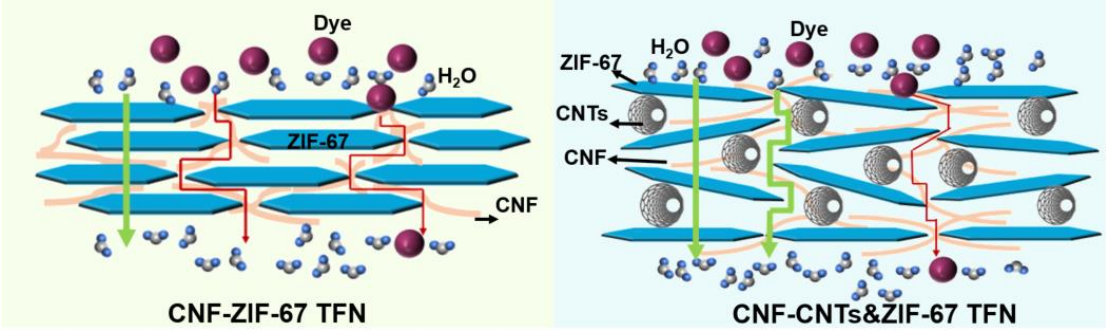

1. Introduction

Since William Perkin's first synthesis of organic red dyes in 1865, the dye synthesis industry has experienced rapid and continuous development [1]. Dyes have greatly enriched the world with vibrant colors. However, the excessive discharge of printing and dyeing wastewater into the environment has become a major challenge for human health [2], especially organic dyes, posing a significant challenge to the purification process due to their resistance to biodegradation [3, 4]. Compared to conventional methods like advanced oxidation processes [5, 6], adsorption [7, 8], biological treatment [9, 10], and coagulation [11, 12], membrane separation offers advantages such as simple operation, high efficiency, low cost, easy maintenance, and good stability, making it a potential alternative for dye wastewater treatment [13]. In recent years, a significant number of studies have focused on the utilization of membranes for dye wastewater treatment [14, 15]. Various materials have been applied in the area, such as metal-organic frameworks (MOFs) [16, 17], graphene oxide (GO) [18, 19], and TiO_2 [20, 21]. However, developing membranes with simultaneously high water flux and dye rejection is always highly desired to improve the competitiveness of membrane technology.

Zeolitic imidazole frameworks (ZIFs) belong to the family of MOFs and are created by combining imidazole salts with central metal ions [22], possessing advantages such as high porosity, large surface area, and tunable morphology. Consequently, ZIFs have been widely used in diverse fields, including gas adsorption, separation, storage, catalysis, and sensing [23-26]. Notably, ZIF-67 and ZIF-8 have attracted significant attention in the field of dye separation due to their unique structure and outstanding chemical stability [27-29].

Currently, extensive research has been conducted on the utilization of ZIFs membranes for dye separation. Various ZIFs-based membranes, such as the PVDF-ZIF-67 composite membrane with excellent separation performance towards triarylmethane dyes [30], in-situ freeze-drying-assisted growth of ZIF-8 composite membranes [31],

modified ZIF-8 membranes [32-34], bimetallic UIO-66@ZIF-8 dual-layer membranes [35], and ZIF-67 in-situ sulfurized CoSx thin-film nanocomposite (TFN) membranes [36], have been developed for dye separation. It is worth noting that in many of those studies, ZIFs were in the form of particles or cubic crystals, thus a thicker selective layer is needed to achieve satisfactory retention rates. However, this frequently leads to decreased water permeance, as observed in the previously mentioned reports, where dye rejection surpasses 95% but permeance falls below 50 $L \cdot m^{-2} \cdot h^{-1} \cdot bar^{-1}$, or even lower [35, 37, 38].

It is well-known that water permeance is a function of selective layer thickness, and thinner membranes can exhibit higher water permeate flux [39]. 2D materials, known for their slender thickness and ordered stacking structures, have attracted much attention in fabricating ultra-thin membranes with exceptional flux [40, 41]. However, membranes composed solely of 2D materials normally possess narrow interlayer gaps, resulting in low water permeance [42-44]. To overcome this challenge, incorporating 1D nanofibers into 2D nanosheets to form interlayer channels appears to be a viable solution. Zhang et al. [45] incorporated Multi-walled carbon nanotubes(MWCNTs)-COOH into the GO interlayer to form GO-MWCNTs-COOH composite membranes. The obtained composite membrane exhibited a ten-fold increase in water permeate flux while the methylene Blue rejection rate was well-maintained. Likewise, the introduction of MWCNTs within layered double hydroxide (LDH) interlayers [46], and the integration of cellulose nanofibers (CNFs) into GO interlayers [47] to form composite membranes resulted in greatly enhanced permeate flux. These findings clearly show that the introduction of 1D nanofibers (e.g., CNTs) into 2D materials can effectively facilitate water molecule transport while rejecting the pollutants.

Inspired by the above research, in the current work, 2D ZIF-67 was synthesized, and two 1D nanofibers (i.e., CNF and CNT) were simultaneously introduced into ZIF-67 to improve the overall wastewater separation performances. CNF serves to bridge the gaps between the ZIF-67 nanosheets, whereas the interlayer formed by CNTs and ZIF-67 functions as a water transport pathway, leading to significant enhancement in water

permeance. Porous polyethersulfone (PES) was selected as porous support for the TFN membranes. The obtained TFN membranes were thoroughly characterized using various techniques, such as SEM, FTIR, and XRD. The effectiveness of the TFN membranes in removing three dyes (Rhodamine B, Methylene Blue, and Direct Red 80) from the water was evaluated in terms of pollutant removal efficiency. Furthermore, the long-term stability of the membranes was also investigated.

2. Experimental

2.1. Materials

$Co(NO_3)_2 \cdot 6H_2O$ (AR), 2-Methylimidazole (LR), anhydrous ethanol (AR), graphitized multi-walled carbon nanotubes (purity >99.9%, inner diameter: 3-5 nm, outer diameter: 8-15 nm, length: ~50 μm), were purchased from Shanghai Aladdin Biochemical Technology Co., Ltd. Carboxylated nanocellulose fibers (length: 2 μm, 1.14 wt.% dispersion in water), Methyl Blue (BS), Rhodamine B (AR), Direct Red 80 (AR) were purchased from Shanghai McLin Biochemical Technology Co., PES (pore size 0.22 μm, diameter 50 mm) was purchased by Titan Instruments Discovery Platform. All the chemicals were used without further purification.

2.2. Synthesis of 2D ZIF-67

0.1455 g of Co $(NO_3)_2 \cdot 6H_2O$ and 0.4905 g of 2-methylimidazole were dissolved in 100 mL of deionized (DI) water separately. The two solutions were then mixed into a flask and stirred at room temperature for 20 minutes. Afterward, the mixture was evenly transferred into centrifuge tubes, and the centrifuge speed was set to 10,000 rpm for 10 minutes. After the centrifugation, the supernatant was discarded, and the solid at the bottom of the centrifuge tube was retained. The solid was washed with DI water. This centrifugation and cleaning process was repeated two times. Finally, the solids at the bottom were dispersed in a glass tube filled with water and sonicated for 2 min to obtain an approximate concentration of 0.0050 g/ml of ZIF-67 dispersion.

2.3. Fabrication of TFNs

2.3.1. CNF/ZIF-67 membranes

0.1500 g of CNF was dispersed in 100 mL of DI water and sonicated for 30 minutes. The ZIF-67 dispersion solution was added to the CNF dispersion and sonicated for 2 minutes. CNF- ZIF-67 TFN has fabricated via vacuum filtration the dispersion onto a porous PES support. The MOF loading was calculated via equation (1) [48]:

$$w = \left(\frac{y}{x+y}\right) \times 100\% \quad (1)$$

In which *x* represents the mass of CNF (g), and *y* represents the mass of ZIF-67 (g).

2.3.2. CNF-CNTs membranes

0.1500 g of CNF was dispersed in 100 mL DI water by sonication for 30 minutes. Next, a certain mass of CNTs was also dispersed in 100 mL DI water by sonication for 4 hours. Subsequently, mix the CNF dispersion and CNTs dispersion and subject them to 2 minutes of sonication to prepare the casting solution. Finally, vacuum filtration was employed to deposit the TFN dispersion onto a PES support, yielding the CNF-CNTs TFN. The calculation of the loading level is given by equation (2) [48]:

$$w = \left(\frac{z}{x+z}\right) \times 100\% \quad (2)$$

In which *x* represents the mass of nanocellulose (g), and *z* represents the mass of CNTs (g).

2.3.3. CNF-CNTs/ZIF-67 membranes

0.1500 g of CNF was dissolved in 100 ml DI water and sonicated for 30 minutes to prepare a CNF dispersion. Then, 0.0004 g of CNTs was taken and sonicated for 4 hours in 100 mL DI water. Afterward, the CNT dispersion was mixed with the CNF dispersion. 60 mL of ZIF-67 dispersion was added into the above mixture and sonicated for 5 min to obtain the membrane casting solution. Finally, the dispersion of the TFN was filtered

onto a PES support using a vacuum filtration method, resulting in a CNF-CNTs/ZIF-67 TFN.

2.4. Membrane characterization

The chemical structure and surface chemical bonds of the membrane samples were analyzed using a Frontier Fourier-transform infrared (FTIR, PerkinElmer) spectrometer within a wavelength range of 4000-650 cm^{-1}.

The morphology of the TFNs was observed using a field emission scanning electron microscope (FESEM, Nova Nano SEM 450, FEI, USA). The cross-sectional samples were prepared by liquid nitrogen quenching, and all samples were gold-coated for 80 s before the test.

The composition and crystalline structure of the samples were observed using an X-ray diffractometer (XRD, Ultima IV, Rigaku, Japan) with a copper target and a wide-angle diffraction. The scanning range was 5-70°, the scanning speed was 5 °/minute, and the step size was 0.02°.

2.5. Wastewater treatment performance measurement

The performance of the TFN was tested using a capped-end filtration system. During the testing process, a TFN membrane was placed in the membrane cell, and a dye solution with a certain concentration was added to a tank as the feed solution. The feed pressure was controlled by a nitrogen gas cylinder. The dye concentration of the solution before and after TFN filtration was measured using a UV spectrophotometer (T3200, Shanghai Youke Instrument Co.).

The permeate flux of the TFN per unit pressure can be calculated using equation (3) [49]:

$$J = \frac{\mathrm{V}}{\mathrm{A}\cdot\Delta\mathrm{t}\cdot\Delta\mathrm{P}} \quad (3)$$

In which J ($L\cdot m^{-2}\cdot h^{-1}\cdot bar^{-1}$) represents the permeate flux, V (L) represents the volume of permeate collected during a certain time interval Δt (h), and A (m^2)

represents the effective membrane area. ΔP (bar) represents the pressure difference across the membranes.

The dye rejection rate is calculated using equation (4) [49]:

$$R = \left(1 - \frac{C_1}{C_0}\right) \times 100\% \quad (4)$$

In which C_0 represents the initial concentration of the dye solution, C_0 represents the initial concentration of the dye solution, and C_1 represents the concentration of the filtrate after filtration.

3. Results and Discussions

3.1. Membrane characterization

The morphology of CNF, CNT, and ZIF-67 was studied using SEM and results are presented in **Figure 1**. **Figure 1 (a)** shows the SEM image of CNF, exhibiting a continuous fibrous structure consistent with the typical morphology reported in previous studies [50, 51]. The SEM image of CNTs is shown in **Figure 1 (b)**, it reveals a more elongated rod-like structure compared to CNF, which is also commonly reported in different literatures [52, 53]. **Figure 1 (c)** demonstrates the unique 2D morphology of ZIF-67, primarily composed of hexagonal nanoplates with a thickness of 30.08 nm and a planer size is 1~2 μm. It should be noted that the morphology of MOF materials can be influenced by various parameters, including reaction time, metal/organic ligand ratio, and concentration [54, 55]. In the current work, the morphology of ZIF-67 can be tuned by controlling the reaction time, the morphology and size of the obtained ZIF-67 may vary from ultra-thin 2D nanosheet to relatively thicker hexagonal platelets (shown in **SI Figure S1**).

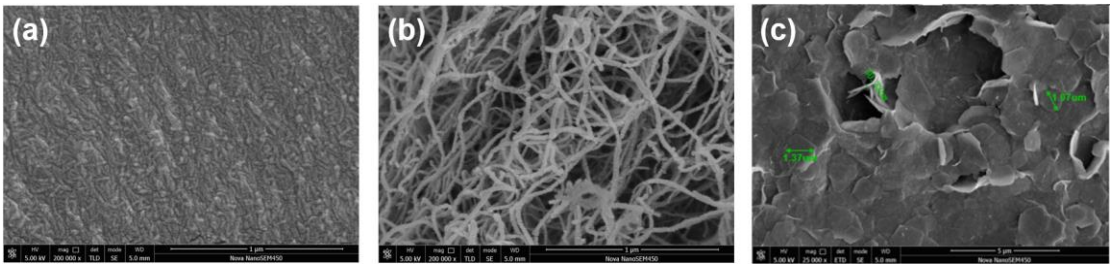

Figure 1. SEM images of CNF(a), CNTs(b), and ZIF-67 nanosheets(c).

The morphology of the TFN membranes was also characterized and presented in **Figure 2**. In **Figure 2 (a)**, the SEM image illustrates the PES porous support, featuring uniformly distributed large pores that do not retain dye molecules but rather provide mechanical strength as support. The surface SEM image of CNF-ZIF-67 with a ZIF loading of 66.67 wt.% was presented in **Figure 2 (b)**, where hexagonal ZIF-67 sheets are observed. Compared to the neat ZIF-67 membranes, the ZIF-67 sheets in CNF-ZIF-67 are tightly packed, forming a complete MOF layer on the surface of the PES support. Moreover, CNF fibers can be observed uniformly dispersed between the ZIF-67 sheets, filling the interstitial gaps and layer surfaces of ZIF-67 nanosheets. The cross-section image demonstrates the well-structured deposition of ZIF-67 layers within CNF-ZIF-67 TFN membranes. Conversely, the pure ZIF-67 TFN membranes, without CNF addition, exhibited notable interlayer voids and fractures (shown in **Figure S2**). These findings provide clear evidence that incorporating CNF fibers into the 2D ZIF-67 matrix significantly improves the stacking and interlayer behavior of the nanosheets, potentially leading to different transport properties.

The morphology of CNF-CNTs incorporated TFN with 0.3 wt.% CNT was also characterized and presented in **Figure 2 (c)**. The surface image shows that the CNTs intersect with CNF nanofibers and form a uniform layer without detectable pores via SEM. Similarly, in the cross-section image, a close intersection between CNTs and CNF is observed, resulting in a compact selective layer. Moreover, **Figure S3** demonstrates that as the loading amount of CNTs increases, CNTs tend to aggregate and intertwine, potentially leading to the formation of non-selective interfacial gaps within the TFNs.

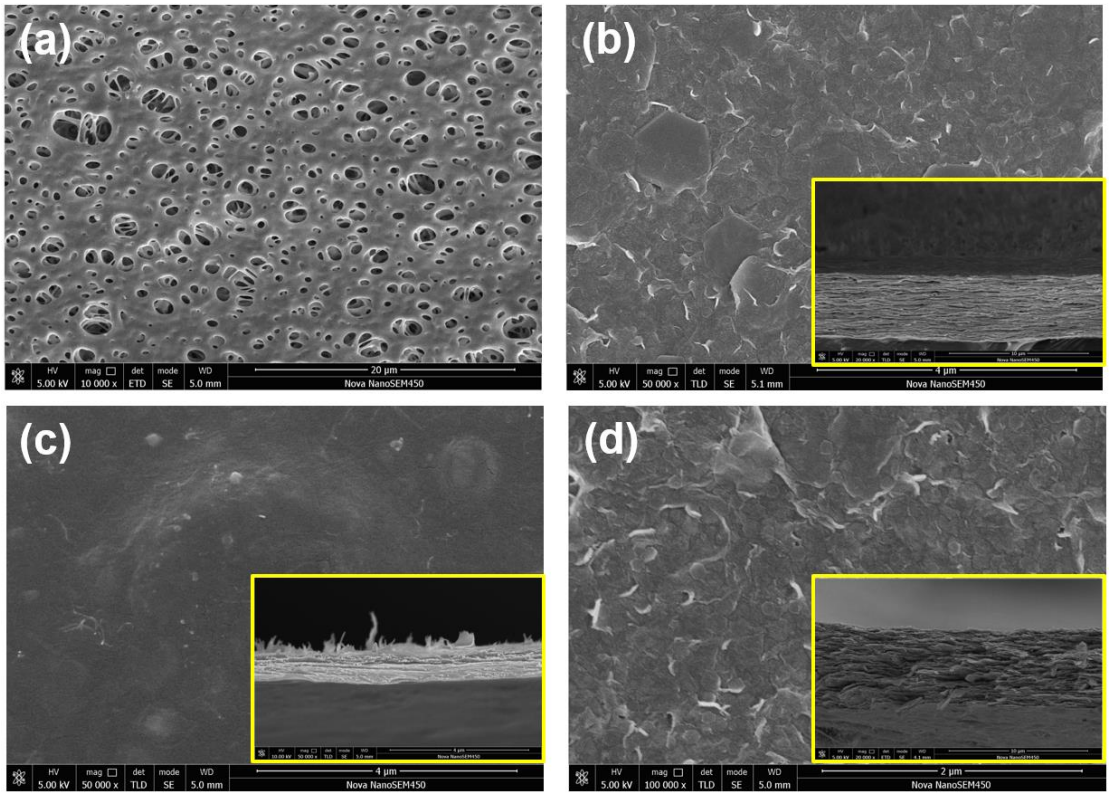

Figure 2. Surface and cross-sectional morphology of TFNs: (a) PES; (b) CNF-ZIF-67 66.67 wt.%; (c) CNF-CNTs 0.3 wt.%; (d) CNF-CNT/ZIF-67 (0.3 wt.% CNTs and 66.67 wt.% ZIF-67).

CNF-CNTs/ZIF-67 TFN was prepared with a ZIF-67 loading of 66.67 wt.% and a CNTs loading of 0.3 wt.%. **Figure 2 (d)** presents the surface image of CNF-CNTs/ZIF-67 TFN membranes. The cross-section image of CNF-CNTs/ZIF-67 TFN membranes reveals a denser structure compared to CNF/ZIF-67 TFN, with a well-arranged distribution of ZIF-67 and uniformly dispersed CNTs. Additionally, after the addition of CNTs, large hexagonal-shaped ZIF-67 nanosheets were not observed on the TFN surface, but instead, a smaller and denser structure was observed. This phenomenon could be attributed to two possible reasons: Firstly, during the ultrasonication process, there might be collisions between ZIF-67 and CNTs, leading to reduced ZIF-67 size [56-59]. Secondly, the introduction of CNTs may form CNTs interlayers, which contribute to the improvement of the stacking structure of ZIF-67 nanosheets [60].

The FTIR and XRD results of the membranes are shown in **Figure 3**. In the FTIR spectrum presented in **Figure 3 (a)**, two absorption peaks at 1580 cm^{-1} and 1487 cm^{-1}

correspond to the C=C bonds in the benzene rings of PES, indicating the skeletal vibrations of the benzene rings. The absorption peak at 1241 cm^{-1} corresponds to the stretching vibration of the C-O-C bonds in PES support. The absorption peak at 1153 cm^{-1} corresponds to the stretching vibration of the O=S=O bonds in PES [61, 62]. The peaks at 1600 cm^{-1} and 1288 cm^{-1} are attributed to the N-H bond in the 2-methylimidazole ring and the Co-N bond in ZIF-67 nanosheets [63], shown in **Figure S4 (a)**. However, it is worth noting that due to the high intensity of peaks from the PES support layer, the peaks from CNF, ZIF-67, and CNTs are not fully visible in the FTIR spectra of the TFNs. **Figure S4 (a)** and **Figure S5 (a)** exhibit the same peak positions.

Figure 3 (b) shows the XRD results of the TFN membranes. Distinctive peaks corresponding to ZIF-67 and CNTs can be observed in CNF-CNTs/ZIF-67, CNF-CNTs 0.3 wt.%, and CNF/ZIF-67 66.67 wt.% TFNs. Additionally, in **Figure S4 (b)** and **Figure S5 (b)**, with an increase in the loading of ZIF-67 and CNTs in the TFNs, the peaks attributed to ZIF-67 and CNTs become increasingly evident, indicating the preservation of the structure of ZIF-67 and CNTs in the TFNs.

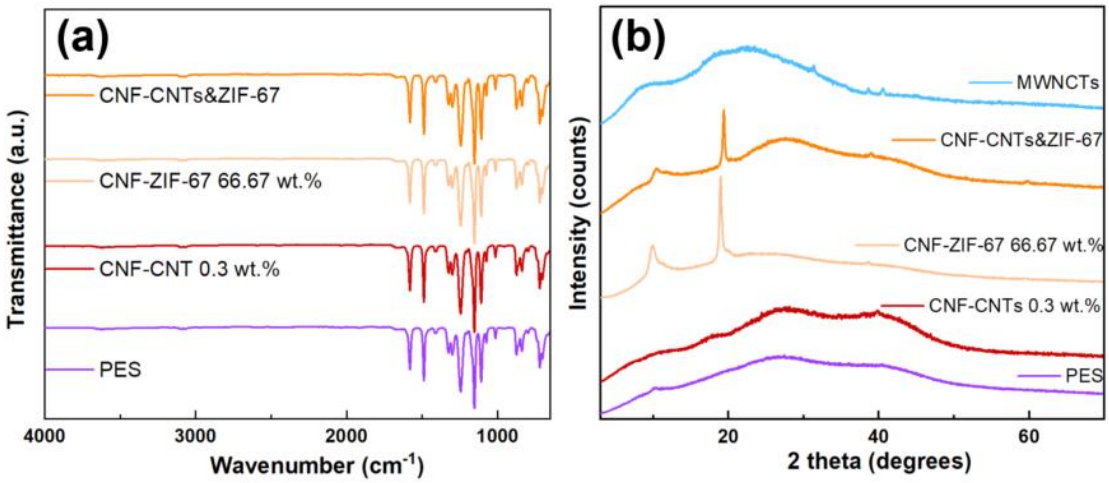

Figure 3. FTIR spectrum (a) and XRD curve (b) of the TFN membranes with different CNF and CNT content.

3.2. Dye separation performances

3.2.1. Dye separation performances of different TFN membranes

Dye separation performances of the obtained TFN membranes (i.e., CNF/ZIF-67, CNT/ZIF-67, and CNF-CNT/ZIF-67) were evaluated and results are presented in **Figure 4**, **Figure 5,** and **Figure 6**.

Figure 4 illustrates the separation performance of CNF/ZIF-67 TFN membranes with different ZIF-67 loadings. It can be observed that as the loading of ZIF-67 increases in the TFN membranes, water permeance gradually reduced, especially when the ZIF-67 content increased to 66.6 wt.%, the water flux dramatically reduced from ~300.0 $L \cdot m^{-2} \cdot h^{-1} \cdot bar^{-1}$ to lower than 100.0 $L \cdot m^{-2} \cdot h^{-1} \cdot bar^{-1}$. Meanwhile, the dye rejection was greatly improved from 22.0% and 13.0% to 96.8% and 93.3% for Methyl Blue, and Direct Red 80 respectively. The reason may be that with the increase of ZIF-67 loading, the stacking structure becomes more pronounced (as shown in **Figure S2**), and the retention of dye molecules becomes more intense, which leads to an increase in rejection. However, the higher content of ZIF-67 nanosheets will also increase the mass transfer resistance of water molecules, which consequently makes the permeance decrease. It is worth mentioning that when the loading of ZIF-67 reaches 100 wt.%, the permeance of the TFNs slightly increases, but the rejection rate significantly decreases. This observation proves the CNF plays a crucial role in filling the gaps between the nanosheets and regulating the structure [64]. Furthermore, SEM results also similarly confirmed the presence of voids between the layers of ZIF-67 nanosheets in the absence of CNF (shown in **Figure S2 (f)**).

In addition, it is also found that the water permeances are slightly different for different dyes, the possible reason can be that the dyes with different properties (e.g., molecular size and shape, molecular polarity, molecular structure) also play a role in the water permeation process, thus leading to the diversity of the water permeance, similar phenomena have been also reported in many different literatures [37, 65-67].

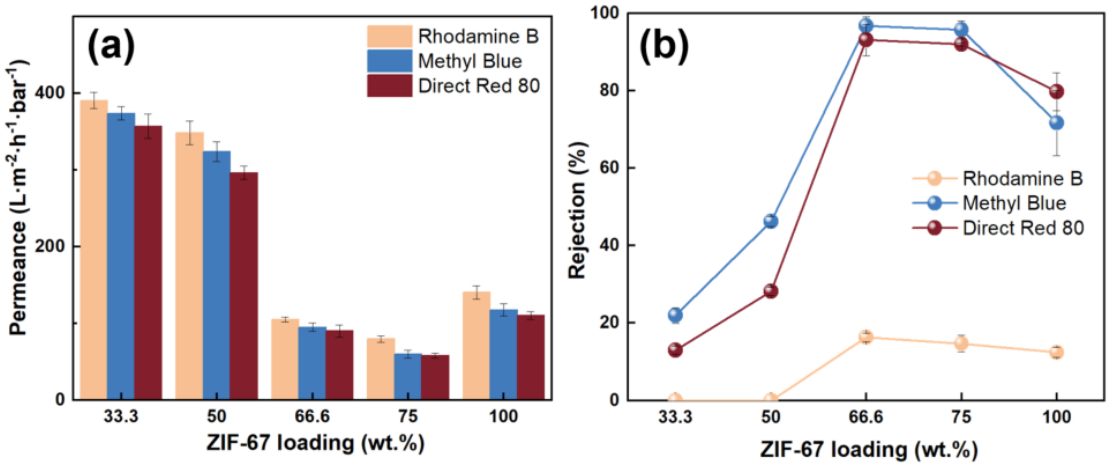

Figure 4. Dye separation performance of CNF-ZIF-67 in different loadings, (a) Water permeance; (b) Rejection.

Figure 5 illustrates the dye separation performance of TFN with different CNTs loadings. It can be observed that the pure CNF membrane exhibits low retention rates for all three dyes, which were lower than 10%. With the increment of CNTs loading in the membranes, the permeance generally increases. However, the rejection rates of the three dyes initially increase and then decrease. At a CNTs loading of 0.3 wt.%, the TFN shows significantly improved rejection rates for all three dyes, particularly for Direct Red 80, where the rejection reaches 87.39%, which is nearly 9 times higher than that of the pure CNF TFN (the rejection is 9.84%). This phenomenon suggests that the addition of CNTs and the crossover of CNFs form fine molecule channels for water and have a certain obstructing effect on dye molecules [68].

However, due to the size difference between CNTs and CNF, CNTs tend to form agglomerates in the membrane with increasing loading, which was also clearly observed in the SEM images of CNF-CNTs shown in **Figure S3**. This leads to possible unobserved cross-slits, which result in higher permeance and lower rejection. In addition, it can be observed that at suitable loadings (0.3 wt.% and 0.5 wt.%), the rejection of Direct Red 80 is much higher than the other two dyes. The reason for this difference may be related to the prominent molecular weight and molecular size of Direct Red 80, as shown in **Table 1.**

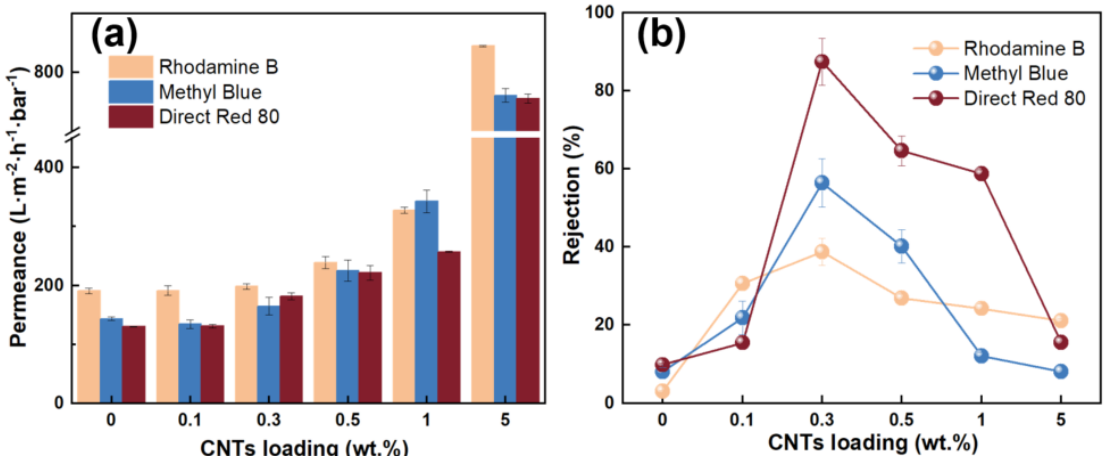

Figure 5. Dye separation performance of CNF-CNTs TFN in different loadings, (a)Water permeance; (b) Rejection.

From the dye removal experimental results shown in **Figure 4** and **Figure 5**, both CNF/ZIF-67 and CNF-CNT membranes exhibit improved dye removal efficiency compared to the neat membranes. On the other hand, for both cases, the water permeance and dye rejection rate still have room for improvement.

Therefore, we selected the optimal loading levels of ZIF-67 (66.67 wt.%) and CNTs (0.3 wt.%) from the previous tests and combined them to prepare CNF-CNTs/ZIF-67 TFN for dye removal. The results are shown in **Figure 6**. Compared to the neat ZIF-67 membranes, introducing CNF nanofibers into the ZIF 67 matrix resulted in slightly reduced water flux but a much higher dye rejection rate. A combination of CNF-CNT nanofibers can also result in membranes with water permeance and a higher Direct Red 80 rejection rate, but the overall separation performance is still not attractive (the rejection rate was 87.4%). On the other hand, when both nanofibers were introduced into the ZIF-67 matrix, the permeance and dye rejection rate improved simultaneously. For instance, the retention rates of Methyl Blue and Direct Red 80 for the CNF-CNTs/ZIF-67 TFN are 95.1% and 96.3%, respectively, 1.32 and 1.20 times higher than the neat ZIF-67 membranes. Moreover, for the removal of Direct Red 80 from water, the permeance of the CNF/ZIF-67 TFN is only 94.0 $L \cdot m^{-2} \cdot h^{-1} \cdot bar^{-1}$, whereas the permeance of the CNF-CNTs/ZIF-67 TFN increases to 170.4 $L \cdot m^{-2} \cdot h^{-1} \cdot bar^{-1}$. This increase in permeance can possibly be attributed to the introduction of CNTs, which enhances the looseness and roughness of the separation

layer, thereby accelerating the transport of water molecules, as shown in **Figure 7**.

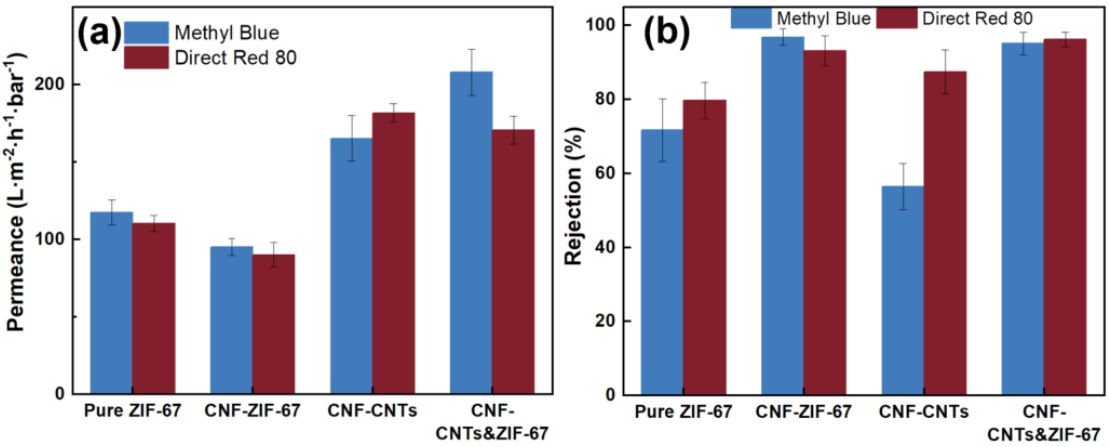

Figure 6. Comparison of dye separation performance of different TFNs: (a)Water permeance; (b) dye rejection.

To explain the substantial improvement in water permeance observed when CNF, CNTs, and ZIF-67 are combined, we propose the following explanation, as depicted in **Figure 7**. In CNF-ZIF-67 TFNs, the stacking of ZIF-67 layers is relatively tight. While this contributes to an increase in dye retention rate, it negatively impacts water molecule transport due to the compact interlayer structure, leading to a reduction in water transport pathways. In CNF-CNTs TFNs, the staggered structure of CNFs effectively enhances the water permeance. Nevertheless, **Figure S3** demonstrates that the presence of partially self-crossing CNTs can lead to the formation of larger intersecting structures, causing a reduction in the dye rejection rate. In CNF-CNTs/ZIF-67 TFNs, several factors contribute to improved water permeance. Firstly, CNTs modify the interlayer transport channels and create enlarged channels between ZIF-67 and CNT layers, facilitating rapid diffusion and migration of water molecules absorbed on the membrane surface [18, 46, 69, 70]. Secondly, the hydrophobic nature of CNTs provides a frictionless pathway for fast water molecule migration [60]. Additionally, the ZIF-67 layers, with the presence of CNF and CNTs, fill the non-selective gaps between the nanosheets and the intersecting structures of CNF-CNTs, leading to enhanced dye retention. As a result, CNF-CNTs/ZIF-67 TFN exhibits improved water permeance and dye retention rate.

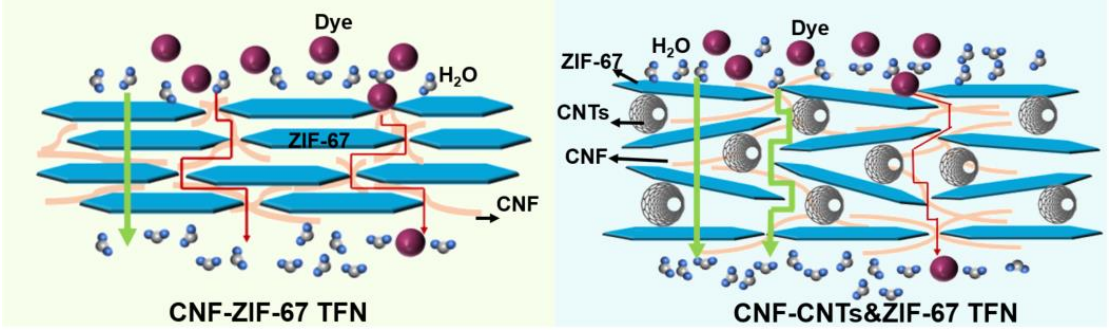

Figure 7. Schematic diagram of the passage of the dye through CNF-ZIF-67 TFN and CNF-CNTs/ZIF-67 TFN

The dye rejection in TFNs is influenced not only by the stacking structure and channels of ZIF-67 but also by the properties of the dyes themselves, including their molecular size (molecular weight), structure, and polarity [49, 65, 71]. The properties of Rhodamine B, Methyl Blue, and Direct Red 80 are provided in **Table 1**, and their chemical formulas are shown in **Figure S6**.

Table 1. Properties of Different Dyes

Dye Type	Molecular Weight (Size)	Structure	Polarity	Ref
Rhodamine B	479 (1.8 nm)	Symmetrical	Cationic dyes	[72]
Methyl Blue	799 (2.36 nm×1.74 nm)	Symmetrical	Anionic dyes	[65]
Direct Red 80	1373 (collective ~5.6 nm)	Linear chain-like	Anionic dyes	[73]

In this study, nearly all TFNs exhibited significantly low dye rejection rates for Rhodamine B (<20%). This can be attributed to the significantly smaller molecular weight and volume of Rhodamine B (479, 1.8 nm) compared to the other two dyes, which have molecular weights of 799 (2.36×1.74 nm) and 1373 (~5.6 nm), respectively. The smaller molecular volume of Rhodamine B may make it easier for the dye to pass through the selective layer of TFNs, directly leading to a lower retention rate. Furthermore, we observed that in certain TFNs prepared, Methyl Blue, which has a relatively smaller molecular weight, displayed a higher rejection rate compared to Direct Red 80. This could be attributed to differences in the molecular structure. The chemical structures of dyes are shown in **Figure S6**. During the dye separation performance test, two possible scenarios may arise when Direct Red 80 traverses the selective layer. In one scenario, the molecular orientation is

perpendicular to the pore direction, and the molecular dimensions surpass the pore size, leading to dye retention. In another scenario, the chain-like structure of Direct Red 80 may align parallel to the pore direction, making it relatively easier for the dye molecules to pass through the pores, resulting in a lower retention rate. However, in the case of Methyl Blue, its nonlinear symmetrical structure enables it to exist as a compact unit, effectively eliminating the possibility of the mentioned scenarios.

However, the electrical properties did not seem to have a significant effect on the retention of dyes. In the TFN membranes developed in the current study, the ZIF-67 stacking layer was mainly used to provide the retention separation performance for dyes. In addition, as shown in SEM images, the surface of the TFN membrane was covered with ZIF-67, and CNTs and CNF were mainly interspersed with ZIF-67 interlayers and interstitials. There is many literatures reporting that ZIF-67 has a positive zeta potential and thus the surface is normally positively charged [65, 74-76]. However, in this study, the retention rate of cationic dye Rhodamine B by TFN was always at a low level (not more than 20%), denoting that the positive repulsive effect was not obvious in the ZIF-67-based TFN membrane, therefore, the Gibbs-Donnan effect did not play a major role in the CNF-CNT/ZIF-67 TFN membranes.

In the developed TFN membranes, CNTs changed the interlayer transport channels and formed expanded channels between the ZIF-67 and CNT layers, which facilitated the rapid diffusion and migration of water molecules absorbed at the membrane surface, resulting in a much higher water permeance of CNF-CNTs/ZIF-67 TFNs. In addition, the size and structure of the dye molecule is an important influence on the rejection rate of the TFN membrane.

3.2.2. Effect of pressure

The best-performing TFNs, namely CNF-CNTs/ZIF-67 (66.6 wt.% ZIF-67,0.3 wt.% CNTs), CNF-CNTs 0.3 wt.%, and CNF/ZIF-67 66.6 wt.% TFNs were selected for dye separation performance testing under variable pressures to study the effect of pressure. **Figure 8 (a)** illustrates the water permeance of the CNF/ZIF-67 TFN as a function of

the operating pressure. With increasing feed pressure, the permeance exhibits a significant increase. At an operating pressure of 1 bar, the permeance was around 100 $L \cdot m^{-2} \cdot h^{-1} \cdot bar^{-1}$. When the feed pressure is raised, the permeance significantly increases to around 200.0 $L \cdot m^{-2} \cdot h^{-1} \cdot bar^{-1}$. It is interesting to see that the water permeance obtained at 3 bar is slightly lower than the value obtained with a feed pressure of 2 bar, potentially due to a more compact structure under high feed pressure conditions. The impact of operating pressure on the rejection rate of the TFN is shown in **Figure 8 (b)**. For all three tested dyes, increasing feed pressure leads to an increment in dye rejection rate, 96.8% and 93.5% were documented as the highest rejection rates for Methylene Blue and Direct Red 80, respectively. The reason for the higher dye rejection rate was consistent with the water permeance, which is possibly due to more compacted ZIF-67 layer packing under higher feed pressure conditions.

Figure 8 (c) and **(d)** present the dye removal results of CNF-CNTs 0.3 wt.% membranes as a function of operating pressure. Interestingly, different from the CNF/ZIF-67 membranes, the water permeance of CNF-CNT membranes reduced with increased feed pressure. With a feed pressure of 1 bar, the TFN achieves the highest permeances, which were 198.5, 165.2, and 181.7 $L \cdot m^{-2} \cdot h^{-1} \cdot bar^{-1}$ and reduced to 151.4, 121.1, and 113.7 $L \cdot m^{-2} \cdot h^{-1} \cdot bar^{-1}$ at 3 bar, respectively. As the operating pressure increases, the permeance reduces gradually. A possible reason can be the CNF-CNT TFN membrane is more porous than the CNF/ZIF-67 membrane, and as the external feed pressure increases, the porous structure becomes more compact, impeding the transport of water molecules. Interestingly, the rejection rate also presents a declining trend similar to water permeance. At an operational pressure of 1 bar, the TFN achieves the highest rejection rates for all three dyes: 87.4% for Rhodamine B, 47.0% for Methyl Blue, and 38.8% for Direct Red 80. As the operating pressure increases, the rejection rates decrease continuously.

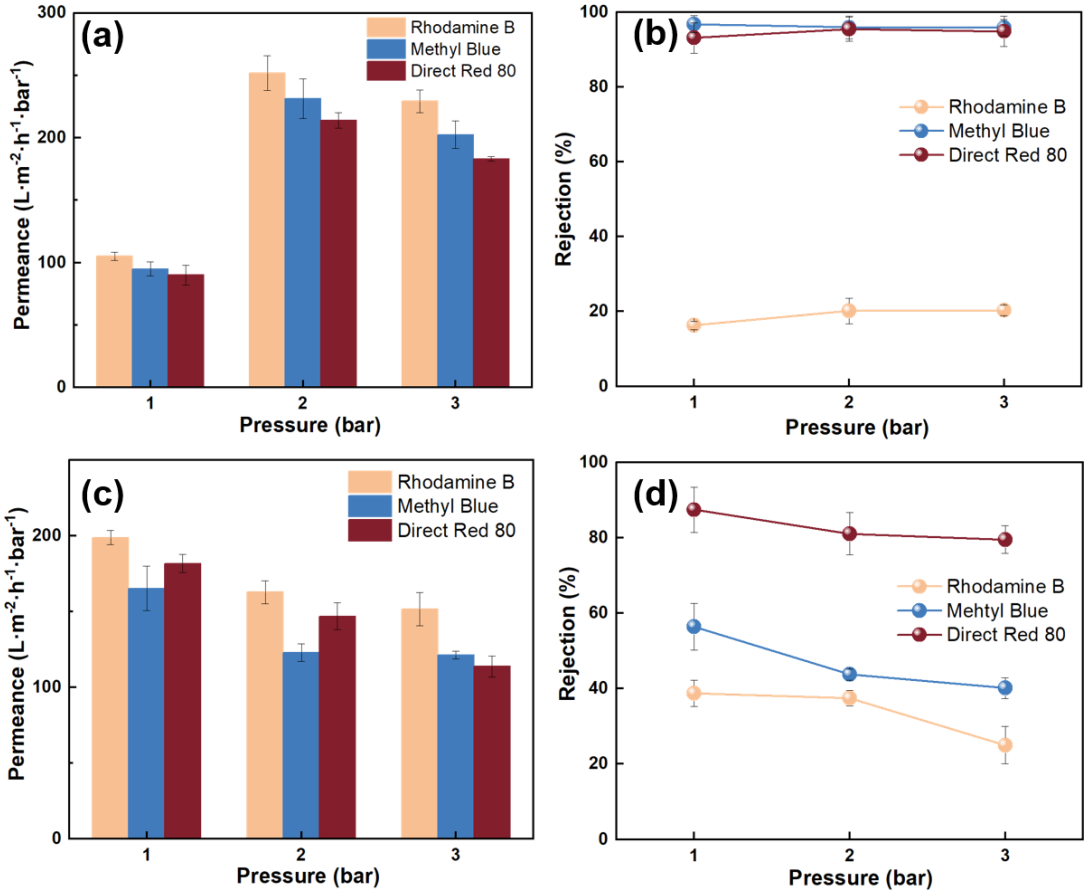

Figure 8. Dye separation performance of different TFNs with different pressures: (a) water permeance of CNF-ZIF-67 66.67wt.% TFN; (a) dye rejection of CNF-ZIF-67 66.67wt.% TFN; (c) water permeance of CNF-CNTs 0.3wt.% TFN; (a) dye rejection of CNF-CNTs 0.3wt.% TFN.

The dye removal performances of the CNF-CNTs/ZIF-67 TFN membranes were tested as a function of operational pressure and results are presented in **Figure 9**. Similar to the two previously discussed TFNs, the flux of CNF-CNTs/ZIF-67 TFN exhibited an increase with increasing operating pressure, as illustrated in **Figure S7**. This phenomenon has also been observed in other studies [36, 77-79]. However, it is found that the water permeance of CNF-CNT/ZIF-67 TFN membranes is different from CNF/ZIF-67 and CNF-CNT membranes. In the experiments involving Methyl Blue and Direct Red 80 separation, the permeance exhibits a similar trend of a slight increase followed by a decrease with increasing operational pressure; a similar phenomenon of increasing and then decreasing permeance with pressure variation has been reported [78]. From **Figure 9 (a)**, it can be observed that when the operating

pressure increased from 1 bar to 2 bar, the permeance of the TFN slightly increased from 397.3, 207.8, and 170.4 $L \cdot m^{-2} \cdot h^{-1} \cdot bar^{-1}$ to 409.7, 209.5, and 181.9 $L \cdot m^{-2} \cdot h^{-1} \cdot bar^{-1}$, respectively. However, as the feed pressure increased to 3 bar, a reduction of the water permeance was observed. Under pressurized conditions, the loose and porous structure becomes compact, thus reducing the transport of water molecules through the membranes [80]. To sum up, the water permeance behavior of the CNF-CNT/ZIF-67 TFN membranes is a combination of CNF-ZIF-67 and CNF-CNT membranes, as the same phenomenon was observed in the above variable pressure tests of CNF-ZIF-67, CNF-CNTs TFNs.

Figure 9 (b) shows the dye rejection rates. It reveals that the TFN exhibits high and stable rejection for Methyl Blue and Direct Red 80 at operational pressures of 1 bar and 2 bar. At 1 bar, the highest rejection rates reached 95.1% and 96.3% for Methyl Blue and Direct Red 80, respectively. Further increasing the feed pressure resulted in a decline in dye rejection, denoting a lower operational pressure is preferable for the CNF-CNT/ZIf-67 TFN membranes.

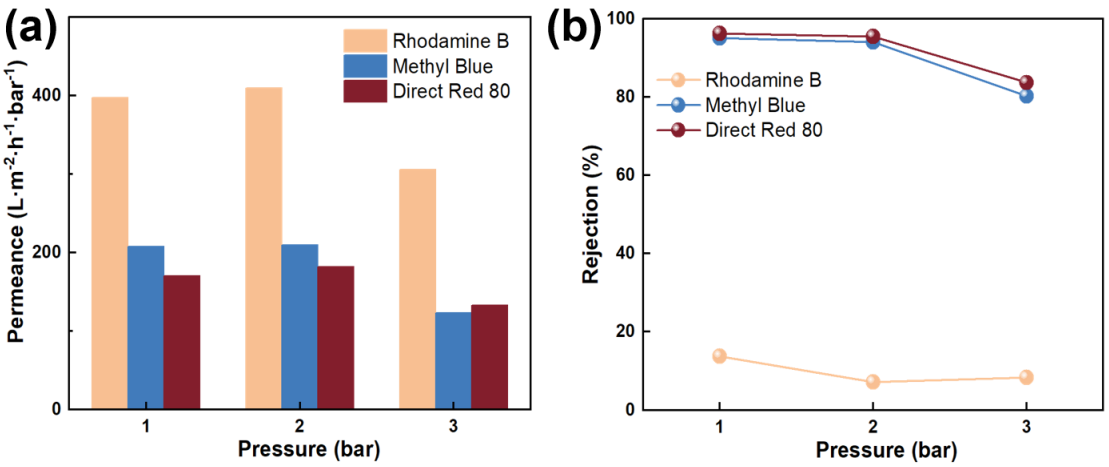

Figure 9. The dye separation performance of CNF-CNTs/ZIF-67 (0.3wt.% CNTs and 66.67wt.% ZIF-67) TFN in different pressures: (a) Water permeance; (b) Rejection.

3.2.3. Long-term stability

The stability of the TFN is crucial for practical applications. In this study, stability tests were performed on the CNF-CNTs/ZIF-67 TFN with a feed pressure of 1 bar. **Figure 10** displays the obtained results. As can be seen from the figure, the prepared TFN

exhibited excellent stability for all three dyes over an 8-hour duration. Direct Red 80 consistently maintained a rejection rate above 95.0%, whereas Methyl Blue showed a consistent rejection rate of approximately 94.0%. In addition, the CNF-CNT/ZIF-67 TFN after the water permeation test was also characterized by SEM and XRD, and the results are shown in **Figure S8**. According to the SEM and XRD results, it can be found the morphology and structure of the TFN membranes were essentially unchanged. High water permeance and dye rejection rate, coupled with excellent durability, make the CNF-CNT/ZIF-67 TFN membranes highly promising for applications in the field of dye removal from wastewater.

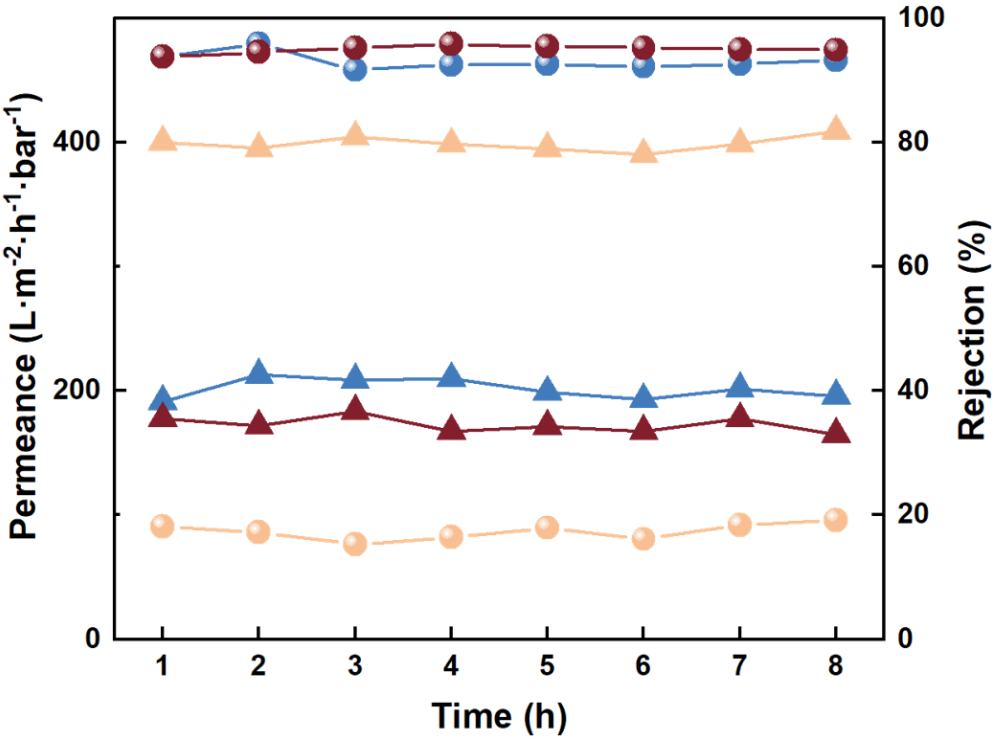

Figure 10. Long-term stability performances of CNF-CNTs/ZIF-67 membranes for different dye separations.

3.2.4. Comparison of membrane performance

A comparison between the separation performance of the TFNs developed in the current study and other reported MOF-based thin films for dye separation was conducted and results are presented in **Table 2** and **Figure 11**. Similar to gas separation membranes, most reported dye removal membranes face a trade-off between permeance and

rejection. Specifically, a membrane with higher permeance usually exhibits a lower dye rejection rate, and vice versa, as shown in **Table 2**. Compared to these literature values, the CNF-CNT/ZIF-67 TFN membranes exhibited both high water flux and high dye rejection rates. For instance, the CNF-CNT/ZIF-67 TFN membranes show a Methyl Blue rejection rate of 95.1%, coupled with a water flux of up to 207.8 $L \cdot m^{-2} \cdot h^{-1} \cdot bar^{-1}$, while other MOF membranes with similar rejection rate hold much lower water permeance [31, 32]. These results clearly demonstrate that the membranes prepared in this study have significant potential for dye removal from wastewater.

Table 2. Comparison of Dye Separation Performance between CNF-ZIF-67 and CNF-CNTs/ZIF-67 TFNs with Existing Studies.

Membranes	Molecular weight	Dye	P($L \cdot m^{-2} \cdot h^{-1} \cdot bar^{-1}$)	Rejection (%)	Ref
PES/PDA-ZIF-8/L	119.16	Isoindoline Yellow A	26.0	96.6	[33]
PES/PDA-ZIF-8/L@DNA	119.16	Isoindoline Yellow A	29.3	96.9	
Al_2O_3-ZIF-8	546.39	Chrome Red	46.6	96.9	[31]
Al_2O_3-ZIF-8	327.33	Methyl Orange	52.0	47.6	
PES-ZIF-8/BMA	696.66	Congo Red	1.1	95.9	[32]
PES-ZIF-8/GMA	696.66	Congo Red	3.2	68.1	
PC/rGO-PAMAM/ZIF-8	479.01	Rhodamine B	30.8	96.8	[81]
MOF-801	696.66	Congo Red	36.2	98.1	[38]
PSF-Ce-UiO-66	681.65	Acid Blue	24.3	97.2	[82]
PSF-Ce-UiO-66	240.21	alizarin	26.9	67.2	
CoSx-ZIF-67	327.33	Methyl Orange	75.4	63.0	[36]
CoSx-ZIF-67	444.45	Tetracycline	61.5	94.1	
CoSx-ZIF-67	11000	Cytochrome C	53.0	96.2	
PVDF-UiO-66-NH2@ZIF-8	319.85	Methylene Blue	36.7	97.0	[35]
HPAN-PEI-ZIF-8	327.33	Methyl Orange	51.0	81.2	[83]
PVDF- NH_2-MIL-53	461.38	Chrome Black T	85.1	81.7	[67]
CNF-CNTs	799.80	Methyl Blue	165.2	56.5	This work
CNF-CNTs	1373.07	Direct Red 80	181.7	87.4	
CNF-ZIF-67	799.80	Methyl Blue	95.0	96.8	
CNF-ZIF-67	1373.07	Direct Red 80	90.0	93.3	
CNF-CNTs/ZIF-67	**799.80**	**Methyl Blue**	**207.8**	**95.1**	
CNF-CNTs/ZIF-67	**1373.07**	**Direct Red 80**	**170.4**	**96.3**	

In addition, the dye removal results are also plotted in **Figure 11**. It can be seen that the CNF-ZIF-67 and PES/CNF-CNTs/ZIF-67 TFN exhibit significantly higher permeance compared to other works while maintaining a high rejection rate for Methyl Blue and Direct Red 80. Specifically, CNF-ZIF-67 demonstrates a permeance of 95.0 $L \cdot m^{-2} \cdot h^{-1} \cdot bar^{-1}$ and a retention rate of 96.8% for Methyl Blue separation, while achieving a permeance of 90.0 $L \cdot m^{-2} \cdot h^{-1} \cdot bar^{-1}$ and a retention rate of 93.3% for Direct Red 80 separation. On the other hand, CNF-CNTs/ZIF-67 exhibit a permeance of 207.8 $L \cdot m^{-2} \cdot h^{-1} \cdot bar^{-1}$ and a retention rate of 95.1% for Methyl Blue separation, and a permeance of 170.5 $L \cdot m^{-2} \cdot h^{-1} \cdot bar^{-1}$ and a retention rate of 96.3% for Direct Red 80. Furthermore, it is worth noting that, compared to other works, our fabricated TFNs are prepared simply through ultrasound and vacuum filtration, making the preparation process straightforward and offering broad prospects for future applications.

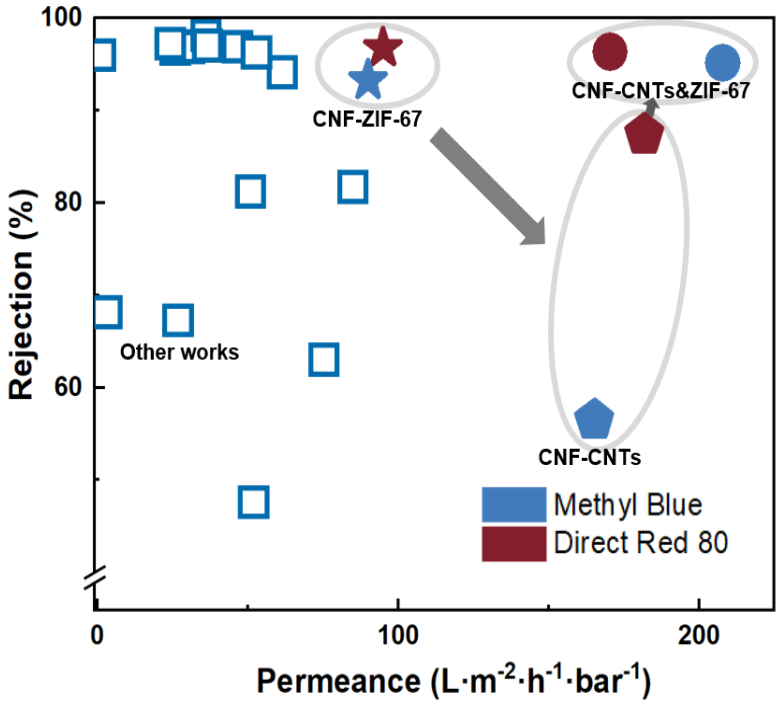

Figure 11. Comparison of CNF-ZIF-67, CNF-CNTs and CNF-CNTs/ZIF-67 TFNs with other works

4. Conclusions

In the current study, a series of TFN membranes were fabricated via the combination of 2D ZIF-67 and two 1D nanofibers, CNF, and CNTs. These TFN membranes were used

for dye separation in wastewater treatment. The results demonstrate that the addition of an appropriate amount of 1D nanofibers into the 2D nanosheet matrix significantly improves dye separation performance. Under optimized conditions, water permeance of up to 207.8 $L \cdot m^{-2} \cdot h^{-1} \cdot bar^{-1}$ with, a rejection rate of 95.1% was documented for Methyl Blue separation, while permeance of 170.5 $L \cdot m^{-2} \cdot h^{-1} \cdot bar^{-1}$ with a retention rate of 96.3% was observed for Direct Red 80, which is much better than most literature values. This study demonstrates the potential of applying two different nanofibers as fillers between 2D nanosheets to improve water permeance while maintaining high rejection rates. These performance-enhancing methods hold great promise for wastewater treatment applications. Further studies can be carried out by employing nanofibers with different functional groups to adjust the nanosheet packing, thus tuning the water and dye molecule transport in the TFN membranes.

Acknowledgments

This work acknowledges the financial support from the Sichuan Science and Technology Program (2021YFH0116), the National Natural Science Foundation of China (No. 52170112).

Reference

[1] I. Holme, Sir William Henry Perkin: a review of his life, work and legacy, Color. Technol., 122 (2006) 235-251,https://doi.org/10.1111/j.1478-4408.2006.00041.x

[2] M. Soylu, Ö. Gökkuş, F. Özyonar, Foam separation for effective removal of disperse and reactive dyes from aqueous solutions, Sep. Purif. Technol., 247 (2020) 116985,https://doi.org/10.1016/j.seppur.2020.116985

[3] S. Servottam, A. Saraswat, M. Eswaramoorthy, C.N.R. Rao, High-Flux lamellar MoSe2 membranes for efficient dye/salt separation, J. Colloid Interface Sci., 646 (2023) 980-990,https://doi.org/10.1016/j.jcis.2023.05.087

[4] S. Zhao, Z. Bai, B. Wang, T. Tian, Z. Hu, Innovative benign-to-design functionalized adsorbents from biomass for rapid azo-dyes separation, Sep. Purif. Technol., 241 (2020) 116633,https://doi.org/10.1016/j.seppur.2020.116633

[5] P. Verma, S.K. Samanta, Microwave-enhanced advanced oxidation processes for the degradation of dyes in water, Environ Chem Lett., 16 (2018) 969-1007,https://doi.org/10.1007/s10311-018-0739-2

[6] P.V. Nidheesh, M. Zhou, M.A. Oturan, An overview on the removal of synthetic dyes from water by

electrochemical advanced oxidation processes, Chemosphere, 197 (2018) 210-227,https://doi.org/10.1016/j.chemosphere.2017.12.195
[7] R. Agarwala, L. Mulky, Adsorption of Dyes from Wastewater: A Comprehensive Review, CHEMBIOENG REV., n/a,https://doi.org/10.1002/cben.202200011
[8] I. Anastopoulos, A. Hosseini-Bandegharaei, J. Fu, A.C. Mitropoulos, G.Z. Kyzas, Use of nanoparticles for dye adsorption: Review, J Dispers Sci Technol., 39 (2018) 836-847,https://doi.org/10.1080/01932691.2017.1398661
[9] I. Ihsanullah, A. Jamal, M. Ilyas, M. Zubair, G. Khan, M.A. Atieh, Bioremediation of dyes: Current status and prospects, J. Water Process. Eng., 38 (2020) 101680,https://doi.org/10.1016/j.jwpe.2020.101680
[10] S. Varjani, P. Rakholiya, H.Y. Ng, S. You, J.A. Teixeira, Microbial degradation of dyes: An overview, Bioresour. Technol., 314 (2020) 123728,https://doi.org/10.1016/j.biortech.2020.123728
[11] F. McYotto, Q. Wei, D.K. Macharia, M. Huang, C. Shen, C.W.K. Chow, Effect of dye structure on color removal efficiency by coagulation, Chem. Eng. J., 405 (2021) 126674,https://doi.org/10.1016/j.cej.2020.126674
[12] P. Cañizares, F. Martínez, C. Jiménez, J. Lobato, M.A. Rodrigo, Coagulation and Electrocoagulation of Wastes Polluted with Dyes, Environ. Sci. Technol., 40 (2006) 6418-6424,https://doi.org/10.1021/es0608390
[13] F. Hu, C. Fang, Z. Wang, C. Liu, B. Zhu, L. Zhu, Poly (N-vinyl imidazole) gel composite porous membranes for rapid separation of dyes through permeating adsorption, Sep. Purif. Technol., 188 (2017) 1-10,https://doi.org/10.1016/j.seppur.2017.06.024
[14] H. Nawaz, M. Umar, I. Nawaz, A. Ullah, M. Tauseef Khawar, M. Nikiel, H. Razzaq, M. Siddiq, X. Liu, Hybrid PVDF/PANI Membrane for Removal of Dyes from Textile Wastewater, Adv Eng Mater., 24 (2022) 2100719,https://doi.org/10.1002/adem.202100719
[15] F. Pan, W. Guo, Y. Su, N.A. Khan, H. Yang, Z. Jiang, Direct growth of covalent organic framework nanofiltration membranes on modified porous substrates for dyes separation, Sep. Purif. Technol., 215 (2019) 582-589,https://doi.org/10.1016/j.seppur.2019.01.064
[16] P. Zhou, J. Cheng, Y. Yan, S. Xu, C. Zhou, Ultrafast preparation of hydrophobic ZIF-67/copper mesh via electrodeposition and hydrophobization for oil/water separation and dyes adsorption, Sep. Purif. Technol., 272 (2021) 118871,https://doi.org/10.1016/j.seppur.2021.118871
[17] K. Chen, P. Li, H. Zhang, H. Sun, X. Yang, D. Yao, X. Pang, X. Han, Q. Jason Niu, Organic solvent nanofiltration membrane with improved permeability by in-situ growth of metal-organic frameworks interlayer on the surface of polyimide substrate, Sep. Purif. Technol., 251 (2020) 117387,https://doi.org/10.1016/j.seppur.2020.117387
[18] L. Huang, Z. Li, Y. Luo, N. Zhang, W. Qi, E. Jiang, J. Bao, X. Zhang, W. Zheng, B. An, G. He, Low-pressure loose GO composite membrane intercalated by CNT for effective dye/salt separation, Sep. Purif. Technol., 256 (2021) 117839,https://doi.org/10.1016/j.seppur.2020.117839
[19] J. Long, Z. Xie, S. Xue, W. Shi, Y. Liu, Highly stable and permeable graphene oxide membrane modified by carbohydrazide for efficient dyes separation, Sep. Purif. Technol., 298 (2022) 121586,https://doi.org/10.1016/j.seppur.2022.121586
[20] L. Zhu, M. Wu, B. Van der Bruggen, L. Lei, L. Zhu, Effect of TiO2 content on the properties of polysulfone nanofiltration membranes modified with a layer of TiO2–graphene oxide, Sep. Purif. Technol., 242 (2020) 116770,https://doi.org/10.1016/j.seppur.2020.116770
[21] L. Zhang, H. Guan, N. Zhang, B. Jiang, Y. Sun, N. Yang, A loose NF membrane by grafting TiO2-

HMDI nanoparticles on PES/β-CD substrate for dye/salt separation, Sep. Purif. Technol., 218 (2019) 8-19,https://doi.org/10.1016/j.seppur.2019.02.018
[22] P. Krokidas, M.B.M. Spera, L.G. Boutsika, I. Bratsos, G. Charalambopoulou, I.G. Economou, T. Steriotis, Nanoengineered ZIF fillers for mixed matrix membranes with enhanced CO2/CH4 selectivity, Sep. Purif. Technol., 307 (2023) 122737,https://doi.org/10.1016/j.seppur.2022.122737
[23] Y. Li, K. Zhou, M. He, J. Yao, Synthesis of ZIF-8 and ZIF-67 using mixed-base and their dye adsorption, Microporous Mesoporous Mater., 234 (2016) 287-292,https://doi.org/10.1016/j.micromeso.2016.07.039
[24] Z. Li, P. Yang, Z. Gao, M. Song, Q. Fang, M. Xue, S. Qiu, A new ZIF molecular-sieving membrane for high-efficiency dye removal, ChemComm., 55 (2019) 3505-3508,https://doi.org/10.1039/C9CC00902G
[25] A. Jaafar, S. El-Husseini, C. Platas-Iglesias, R.A. Bilbeisi, Zeolitic imidazolate framework (AMCD-ZIF) functionalised membrane for the removal of dyes from water, J. Environ. Chem. Eng., 10 (2022) 108019,https://doi.org/10.1016/j.jece.2022.108019
[26] J. Vega, A. Andrio, A.A. Lemus, J.A.I. Díaz, L.F. del Castillo, R. Gavara, V. Compañ, Modification of polyetherimide membranes with ZIFs fillers for CO2 separation, Sep. Purif. Technol., 212 (2019) 474-482,https://doi.org/10.1016/j.seppur.2018.11.033
[27] Y. Liu, D. Lin, W. Yang, X. An, A. Sun, X. Fan, Q. Pan, In situ modification of ZIF-67 with multi-sulfonated dyes for great enhanced methylene blue adsorption via synergistic effect, Microporous Mesoporous Mater., 303 (2020) 110304,https://doi.org/10.1016/j.micromeso.2020.110304
[28] Q. Yang, R. Lu, S. Ren, C. Chen, Z. Chen, X. Yang, Three dimensional reduced graphene oxide/ZIF-67 aerogel: Effective removal cationic and anionic dyes from water, Chem. Eng. J., 348 (2018) 202-211,https://doi.org/10.1016/j.cej.2018.04.176
[29] A. Yeerken, J. Lin, X. Wang, Y. Luo, H. Ma, Fabrication of novel porous ZIF-67/PES composite microspheres and the efficient adsorption of triphenylmethane dyes from water, CrystEngComm, 25 (2023) 1076-1089,https://doi.org/10.1039/D2CE01486F
[30] V. Vatanpour, S. Khorshidi, Surface modification of polyvinylidene fluoride membranes with ZIF-8 nanoparticles layer using interfacial method for BSA separation and dye removal, Mater. Chem. Phys., 241 (2020) 122400,https://doi.org/10.1016/j.matchemphys.2019.122400
[31] K. Ma, N. Wang, C. Wang, Q.-F. An, Freezing assisted in situ growth of nano-confined ZIF-8 composite membrane for dye removal from water, J. Membr. Sci., 632 (2021) 119352,https://doi.org/10.1016/j.memsci.2021.119352
[32] R. Li, J.P. Chen, V. Freger, A new fabrication approach for mixed matrix membrane fabricated with interstitially sealed MOF nanoparticles, J. Membr. Sci., 671 (2023) 121357,https://doi.org/10.1016/j.memsci.2023.121357
[33] M.-y. Zhang, X.-p. Wang, R. Lin, Y. Liu, F.-s. Chen, L.-s. Cui, X.-m. Meng, J. Hou, Improving the hydrostability of ZIF-8 membrane by biomolecule towards enhanced nanofiltration performance for dye removal, J. Membr. Sci., 618 (2021) 118630,https://doi.org/10.1016/j.memsci.2020.118630
[34] C. Gao, P. Zou, S. Ji, Y. Xing, J. Cai, J. Wu, T. Wu, High-flux loose nanofiltration membrane with anti-dye fouling ability based on TA@ZIF-8 for efficient dye/salt separation, J. Environ. Chem. Eng., 11 (2023) 110444,https://doi.org/10.1016/j.jece.2023.110444
[35] Y. Xu, X. Zhao, R. Chang, H. Qu, J. Xu, J. Ma, Designing heterogeneous MOF-on-MOF membrane with hierarchical pores for effective water treatment, J. Membr. Sci., 658 (2022) 120737,https://doi.org/10.1016/j.memsci.2022.120737

[36] H. Sun, N. Wang, X. Li, Q.-F. An, Fabrication of MOF derivatives composite membrane via in-situ sulfurization for dye/salt separation, J. Membr. Sci., 645 (2022) 120211,https://doi.org/10.1016/j.memsci.2021.120211
[37] M. Wu, Y. Sun, T. Ji, K. Yu, L. Liu, Y. He, J. Yan, S. Meng, W. Hu, X. Fan, D. Du, Y. Liu, Fabrication of water-stable MOF-808 membrane for efficient salt/dye separation, J. Membr. Sci., 686 (2023) 122023,https://doi.org/10.1016/j.memsci.2023.122023
[38] F. Yan, J. Yan, Y. Sun, T. Ji, Y. He, X. Guo, Y. Liu, Fabrication of Defect-Engineered MOF-801 Membrane for Efficient Dye Rejection, Eur. J. Inorg. Chem., 26 (2023) e202200679,https://doi.org/10.1002/ejic.202200679
[39] W. Zhang, Y. Qin, W. Shi, Y. Hu, Unveiling the Molecular Mechanisms of Thickness-Dependent Water Dynamics in an Ultrathin Free-Standing Polyamide Membrane, J. Phys. Chem. B., 124 (2020) 11939-11948,https://doi.org/10.1021/acs.jpcb.0c07263
[40] J. Yao, C. Liu, X. Liu, J. Guo, S. Zhang, J. Zheng, S. Li, Azobenzene-assisted exfoliation of 2D covalent organic frameworks into large-area, few-layer nanosheets for high flux and selective molecular separation membrane, J. Membr. Sci., 601 (2020) 117864,https://doi.org/10.1016/j.memsci.2020.117864
[41] T. Liu, H. Zhou, N. Graham, W. Yu, K. Sun, 2D kaolin ultrafiltration membrane with ultrahigh flux for water purification, Water Res., 156 (2019) 425-433,https://doi.org/10.1016/j.watres.2019.03.050
[42] R. Han, X. Ma, Y. Xie, D. Teng, S. Zhang, Preparation of a new 2D MXene/PES composite membrane with excellent hydrophilicity and high flux, RSC Adv., 7 (2017) 56204-56210,https://doi.org/10.1039/C7RA10318B
[43] X. Chen, M. Qiu, H. Ding, K. Fu, Y. Fan, A reduced graphene oxide nanofiltration membrane intercalated by well-dispersed carbon nanotubes for drinking water purification, Nanoscale, 8 (2016) 5696-5705,https://doi.org/10.1039/C5NR08697C
[44] S. Li, W. Gu, Y. Sun, D. Zou, W. Jing, Perforative pore formation on nanoplates for 2D porous MXene membranes via H2O2 mild etching, Ceram. Int., 47 (2021) 29930-29940,https://doi.org/10.1016/j.ceramint.2021.07.166
[45] W.-J. Zeng, C. Li, Y. Feng, S.-H. Zeng, B.-X. Fu, X.-L. Zhang, Carboxylated multi-walled carbon nanotubes (MWCNTs-COOH)-intercalated graphene oxide membranes for highly efficient treatment of organic wastewater, J. Water Process. Eng., 40 (2021) 101901,https://doi.org/10.1016/j.jwpe.2020.101901
[46] Q. Li, P. Song, Y. Yang, Y. Li, N. Wang, Q. An, CNTs Intercalated LDH Composite Membrane for Water Purification with High Permeance, Nanomaterials, 12 (2022) 59
[47] P. Liu, C. Zhu, A.P. Mathew, Mechanically robust high flux graphene oxide - nanocellulose membranes for dye removal from water, J. Hazard. Mater., 371 (2019) 484-493,https://doi.org/10.1016/j.jhazmat.2019.03.009
[48] Z. Qin, X. Feng, D. Yin, B. Xin, Z. Jin, Y. Deng, L. Yang, L. Yao, W. Jiang, C. Liu, Z. Dai, Impact of Humidity on the CO2/N2 Separation Performance of Pebax-MOF Mixed Matrix Membranes, Ind. Eng. Chem. Res., 62 (2023) 14034-14046,https://doi.org/10.1021/acs.iecr.3c02308
[49] Y. Zhang, H. Ye, D. Chen, N. Li, Q. Xu, H. Li, J. He, J. Lu, In situ assembly of a covalent organic framework composite membrane for dye separation, J. Membr. Sci., 628 (2021) 119216,https://doi.org/10.1016/j.memsci.2021.119216
[50] S. Pak, J. Ahn, H. Kim, High performance and sustainable CNF membrane via facile in-situ envelopment of hydrochar for water treatment, Carbohydr. Polym., 296 (2022) 119948,https://doi.org/10.1016/j.carbpol.2022.119948

[51] S. Mohammed, H. M. Hegab, R. Ou, Nanofiltration performance of glutaraldehyde crosslinked graphene oxide-cellulose nanofiber membrane, Chem Eng Res Des., 183 (2022) 1-12,https://doi.org/10.1016/j.cherd.2022.04.039
[52] R.S. Lankone, J. Wang, J.F. Ranville, D.H. Fairbrother, Photodegradation of polymer-CNT nanocomposites: effect of CNT loading and CNT release characteristics, Environ. Sci. Nano., 4 (2017) 967-982,https://doi.org/10.1039/C6EN00669H
[53] A. Khalid, A. Abdel-Karim, M. Ali Atieh, S. Javed, G. McKay, PEG-CNTs nanocomposite PSU membranes for wastewater treatment by membrane bioreactor, Sep. Purif. Technol., 190 (2018) 165-176,https://doi.org/10.1016/j.seppur.2017.08.055
[54] I.E. Khalil, J. Fonseca, M.R. Reithofer, T. Eder, J.M. Chin, Tackling orientation of metal-organic frameworks (MOFs): The quest to enhance MOF performance, Coord Chem Rev., 481 (2023) 215043,https://doi.org/10.1016/j.ccr.2023.215043
[55] N.A. Khan, Z. Hasan, S.H. Jhung, Beyond pristine metal-organic frameworks: Preparation and application of nanostructured, nanosized, and analogous MOFs, Coord Chem Rev., 376 (2018) 20-45,https://doi.org/10.1016/j.ccr.2018.07.016
[56] Y. Okada, N. Oshio, K. Oda, S. Kudoh, Fragmentation of Nanoparticle Agglomerates by Collisions in Supersonic Flows, J. Chem. Eng. Japan., 46 (2013) 530-534,https://doi.org/10.1252/jcej.13we044
[57] S.J. Doktycz, K.S. Suslick, Interparticle Collisions Driven by Ultrasound, Science, 247 (1990) 1067-1069,https://doi.org/10.1126/science.2309118
[58] A. Hadi, J. Zahirifar, J. Karimi-Sabet, A. Dastbaz, Graphene nanosheets preparation using magnetic nanoparticle assisted liquid phase exfoliation of graphite: The coupled effect of ultrasound and wedging nanoparticles, Ultrason Sonochem., 44 (2018) 204-214,https://doi.org/10.1016/j.ultsonch.2018.02.028
[59] T. Prozorov, R. Prozorov, K.S. Suslick, High Velocity Interparticle Collisions Driven by Ultrasound, J. Am. Chem. Soc., 126 (2004) 13890-13891,https://doi.org/10.1021/ja049493o
[60] H. Xu, J. Ma, M. Ding, Z. Xie, Mechanistic insights into the removal of PFOA by 2D MXene/CNT membrane with the influence of Ca2+ and humic acid, Desalination, 529 (2022) 115643,https://doi.org/10.1016/j.desal.2022.115643
[61] J. Lei, Z. Guo, PES asymmetric membrane for oil-in-water emulsion separation, Colloids Surf. A Physicochem. Eng. Asp., 626 (2021) 127096,https://doi.org/10.1016/j.colsurfa.2021.127096
[62] V. Vatanpour, A. Dehqan, A.R. Harifi-Mood, Ethaline deep eutectic solvent as a hydrophilic additive in modification of polyethersulfone membrane for antifouling and separation improvement, J. Membr. Sci., 614 (2020) 118528,https://doi.org/10.1016/j.memsci.2020.118528
[63] S. Feng, M. Bu, J. Pang, W. Fan, L. Fan, H. Zhao, G. Yang, H. Guo, G. Kong, H. Sun, Z. Kang, D. Sun, Hydrothermal stable ZIF-67 nanosheets via morphology regulation strategy to construct mixed-matrix membrane for gas separation, J. Membr. Sci., 593 (2020) 117404,https://doi.org/10.1016/j.memsci.2019.117404
[64] H. Ma, Z. Xie, Y. Liu, Q. Zhang, P. Gong, F. Meng, Y. Niu, C.B. Park, G. Li, Improved dielectric and electromagnetic interference shielding performance of materials by hybrid filler network design in three-dimensional nanocomposite films, Mater. Des., 226 (2023) 111666,https://doi.org/10.1016/j.matdes.2023.111666
[65] F. Sheng, X. Li, Y. Li, N.U. Afsar, Z. Zhao, L. Ge, T. Xu, Cationic covalent organic framework membranes for efficient dye/salt separation, J. Membr. Sci., 644 (2022) 120118,https://doi.org/10.1016/j.memsci.2021.120118
[66] D. Liu, Z. Zhu, Y. Zhao, Y. Chen, Y. Tan, Y. Zhang, Low pressure modified polyamide 6 membrane

for effective fractionation of dyes and NaCl, Sci. Total Environ., 695 (2019) 133908,https://doi.org/10.1016/j.scitotenv.2019.133908
[67] X. Lu, Y. Geng, Z. Jia, Y. Yang, H. Huang, Y. Men, L.A. Hou, In situ syntheses of NH2-MIL-53/PVDF composite membranes for dyes separation, Sep. Purif. Technol., 269 (2021) 118760,https://doi.org/10.1016/j.seppur.2021.118760
[68] A. Noy, H.G. Park, F. Fornasiero, J.K. Holt, C.P. Grigoropoulos, O. Bakajin, Nanofluidics in carbon nanotubes, Nano Today, 2 (2007) 22-29,https://doi.org/10.1016/S1748-0132(07)70170-6
[69] H. Yao, H. Yu, B.Y. Zhang, K. Chen, Q. Yi, H. Xie, X. Hu, T. Tang, Y. Cheng, X. Tao, K. Xu, J.Z. Ou, Approximately 1 nm-sized artificial tunnels in wrinkled graphene-graphene oxide composite membranes for efficient dye/dye separation and dye desalination, Chem. Eng. J., 445 (2022) 136753,https://doi.org/10.1016/j.cej.2022.136753
[70] J.-K. Wu, C.-C. Ye, T. Liu, Q.-F. An, Y.-H. Song, K.-R. Lee, W.-S. Hung, C.-J. Gao, Synergistic effects of CNT and GO on enhancing mechanical properties and separation performance of polyelectrolyte complex membranes, Mater. Des., 119 (2017) 38-46,https://doi.org/10.1016/j.matdes.2017.01.056
[71] X. Feng, D. Peng, J. Zhu, Y. Wang, Y. Zhang, Recent advances of loose nanofiltration membranes for dye/salt separation, Sep. Purif. Technol., 285 (2022) 120228,https://doi.org/10.1016/j.seppur.2021.120228
[72] K. Vinothkumar, M. Shivanna Jyothi, C. Lavanya, M. Sakar, S. Valiyaveettil, R.G. Balakrishna, Strongly co-ordinated MOF-PSF matrix for selective adsorption, separation and photodegradation of dyes, Chem. Eng. J., 428 (2022) 132561,https://doi.org/10.1016/j.cej.2021.132561
[73] Z. Jin, Y. Shen, X. Da, X. Chen, M. Qiu, Y. Fan, Construction of high-performance CeO2 ultrafiltration membrane for high-temperature dye/salt separation, J. Membr. Sci., 637 (2021) 119608,https://doi.org/10.1016/j.memsci.2021.119608
[74] X.-D. Du, C.-C. Wang, J.-G. Liu, X.-D. Zhao, J. Zhong, Y.-X. Li, J. Li, P. Wang, Extensive and selective adsorption of ZIF-67 towards organic dyes: Performance and mechanism, J. Colloid Interface Sci., 506 (2017) 437-441,https://doi.org/10.1016/j.jcis.2017.07.073
[75] G. Hu, W. Zhang, Y. Chen, C. Xu, R. Liu, Z. Han, Removal of boron from water by GO/ZIF-67 hybrid material adsorption, Environ. Sci. Pollut. Res., 27 (2020) 28396-28407,https://doi.org/10.1007/s11356-020-08018-6
[76] Z.-h. Zhang, J.-l. Zhang, J.-m. Liu, Z.-h. Xiong, X. Chen, Selective and Competitive Adsorption of Azo Dyes on the Metal–Organic Framework ZIF-67, Water Air Soil Pollut., 227 (2016) 471,https://doi.org/10.1007/s11270-016-3166-7
[77] R. Ghanbari, A.A. Heidari, H. Mahdavi, Core-shell antibacterial conjugated nanostarch incorporated PVDF membrane for fast and efficient dye separation, J. Environ. Chem. Eng., 11 (2023) 109655,https://doi.org/10.1016/j.jece.2023.109655
[78] X. Ji, Y. Bao, C. Du, Q. Shi, W. Xu, Z. Wang, Two-dimensional MWW-type zeolite membranes for efficient dye separation and water purification, Desalination, 541 (2022) 116023,https://doi.org/10.1016/j.desal.2022.116023
[79] X. Zhang, H. Li, J. Wang, D. Peng, J. Liu, Y. Zhang, In-situ grown covalent organic framework nanosheets on graphene for membrane-based dye/salt separation, J. Membr. Sci., 581 (2019) 321-330,https://doi.org/10.1016/j.memsci.2019.03.070
[80] X. Li, L. Lin, Z. Liu, J. Yang, W. Ma, X. Yang, X. Li, C. Wang, Q. Xin, K. Zhao, A “micro-explosion” strategy for preparing membranes with high porosity, permeability, and dye/salt separation efficiency, J

764 Ind Eng Chem., 119 (2023) 516-531,https://doi.org/10.1016/j.jiec.2022.11.075
765 [81] C. Liu, Y.-L. Tong, X.-Q. Yu, H. Shen, Z. Zhu, Q. Li, S. Chen, MOF-Based Photonic Crystal Film
766 toward Separation of Organic Dyes, ACS Appl. Mater. Interfaces., 12 (2020) 2816-
767 2825,https://doi.org/10.1021/acsami.9b18012
768 [82] U. Nellur, N.S. Naik, R.M. Rego, M. Kigga, G. Arthanareeswaran, M. Padaki, Ce-MOF infused
769 membranes with enhanced molecular sieving in the application of dye rejection, Environ. Sci. Water Res.
770 Technol., 9 (2023) 1216-1230,https://doi.org/10.1039/D2EW00931E
771 [83] L. Yang, Z. Wang, J. Zhang, Zeolite imidazolate framework hybrid nanofiltration (NF) membranes
772 with enhanced permselectivity for dye removal, J. Membr. Sci., 532 (2017) 76-
773 86,https://doi.org/10.1016/j.memsci.2017.03.014
774